Applied Geochemistry 206 (2026) 106899

Contents lists available at ScienceDirect

Applied Geochemistry

journal homepage: www.elsevier.com/locate/apgeochem

# Processes affecting pollution fluxes during the coastal erosion of legacy colliery wastes

Ian T. Burke [a,*], Sebastian J. Pitman [b], James Hodson [a], Lin Niu [a], Fatmah Mohammed [a], Jenni Ilari Skakunova [a], Alex L. Riley [c], Catherine J. Gandy [d], Elliot Whitehead [d], Karen A. Hudson-Edwards [e], Elin Jennings [e], Helen Jay [f], Nick Cooper [g], Adam P. Jarvis [d], William M. Mayes [c]

[a] School of Earth and Environment, University of Leeds, Leeds, United Kingdom
[b] School of Geography Politics and Sociology, Newcastle University, Newcastle Upon Tyne, United Kingdom
[c] School of Environmental Sciences, University of Hull, Kingston upon Hull, United Kingdom
[d] School of Engineering, Newcastle University, Newcastle Upon Tyne, United Kingdom
[e] Camborne School of Mines and Environment and Sustainability Institute, University of Exeter, Penryn, United Kingdom
[f] The National Trust, Swindon, United Kingdom
[g] HaskoningUK Ltd., Newcastle Upon Tyne, United Kingdom

ARTICLE INFO

Editorial handling by:G. Bird

*Keywords:*
Colliery spoil
Potentially toxic elements (PTEs)
Coastal erosion
Particulate dispersion
LiDAR analysis

ABSTRACT

The fate and behaviour of legacy coastal waste deposits are of concern due to the potential for future climate change to increase contaminant fluxes from these sources. During the 20th century 39-47 million $m^3$ of pyritic colliery spoil was dumped onto beaches in County Durham, Northeast England. Distribution of this waste along the coastline produced a 4-6 m high compacted colliery spoil terrace, which extended around 200 m seaward of original shoreline. After the cessation of tipping between 1974 and 1993, ongoing erosion of spoil terraces at these sites has become a source of several potentially toxic elements (PTEs) to coastal ecosystems. The compacted spoil material had an in-situ bulk density of 1.8 (1.2-2.0) t $m^{-3}$ and moisture content of 21 (11-31) wt. % and contained potentially problematic mean concentrations of As (142 mg $kg^{-1}$), Ba (1300 mg $kg^{-1}$), Hg (0.63 mg $kg^{-1}$), Pb (154 mg $kg^{-1}$), and Zn (111 mg $kg^{-1}$). Leaching tests showed that the remobilisation of these PTEs was low across a range of pH, indicating particulate dispersion as the most important pollutant transport mechanism at these sites. However, particle winnowing and density separation occur during spoil erosion. Fe oxide and pyrite grains from the spoil were preferentially retained in adjacent fine sand intertidal sediments, which as a result, also contained high concentrations of PTEs. Analysis of beach volume changes between 2010 and 2023 revealed that approximately 500,000 $m^3$ of spoil was removed by coastal erosion in this period. This equates to median annual fluxes of As (6.6 t $yr^{-1}$), Hg (0.027 t $yr^{-1}$), and Pb (4.6 t $yr^{-1}$), and Zn (4.5 t $yr^{-1}$), which are not trivial when compared to annual fluxes from permitted UK industrial discharges or metal mine discharges in England and Wales. The high flux of As is particularly of concern due to the lack of other significant local sources of this metalloid in Northeast England. Although >95 % of the originally tipped spoil has already been dispersed offshore, approximately 1 million $m^3$ of spoil is currently still present in beach deposits, which will remain a significant source of PTEs to coastal environments for several more decades.

## 1. Introduction

Disposal of pyritic mining wastes into coastal and marine environments has occurred in many locations worldwide (Dold, 2014). Such disposal has been considered advantageous as land is not required for long-term waste storage and a range of deleterious terrestrial impacts (e.g. acid leachates, fugitive dust formation) are avoided (Brunskill, 2012). However, this practice can result in a range of negative marine ecosystem impacts caused by both the smothering effects of dispersed fine-grained material and the release of potentially toxic elements

* Corresponding author.
*E-mail address:* i.t.burke@leeds.ac.uk (I.T. Burke).

https://doi.org/10.1016/j.apgeochem.2026.106899
Received 3 June 2025; Received in revised form 1 May 2026; Accepted 20 May 2026
Available online 23 May 2026

(PTEs) (Edinger, 2012; Vogt, 2012).

It is estimated that 39-47 million $m^3$ of colliery spoil was deposited on beaches adjacent to four coal mines on the Co. Durham Coast, Northeast England during the 20th Century (Pitman et al., 2024; Fig. 1). This waste was reported to have primarily originated as coal washing residue (Cooper et al., 2017; Eagle, 1979) produced as a result of coal beneficiation. Coal washing (density separation of the lower density coal from other higher density components) provides multiple benefits during its combustion, including higher calorific content, lower ash content due to the removal of silicates, and lower $SO_2$ and trace metal emissions (e.g. As, Pb, Cd, Hg) due to the removal of pyrite-S (Chugh and Behum, 2014; Miller, 2015). Thus, the colliery spoils produced by coal washing are typically granular materials composed of waste rock, some coal fragments, and can be enriched in pyrite-S (Wiggering, 1993). After deposition, colliery spoil can be subject to both physical and chemical degradation resulting in compaction (Kent, 1982), and acid generation processes associated with microbially mediated pyrite oxidation (Equations (1)–(3); (Acharya and Kharel, 2020).

$$FeS_2 + 3.5O_2 + H_2O \rightarrow Fe^{2+} + SO_4^{2-} + 2H^+ \quad (1)$$

$$4Fe^{2+} + O_2 + 4H^+ \rightarrow 4Fe^{3+} + 2H_2O \quad (2)$$

$$FeS_2 + 14Fe^{3+} + 8H_2O \rightarrow 15Fe^{2+} + 2SO_4^{2-} + 16H^+ \quad (3)$$

Much of the colliery spoil deposited at the Co. Durham coastline was rapidly transported away from the original tipping locations, resulting in the lateral spread of spoil along a 12 km stretch of coastline and typically around 200 m of seaward shoreline progression (Cooper et al., 2017; Pitman et al., 2024). After deposition the spoil compacted in-situ and formed kilometres long spoil terraces between 4 and 6 m above sea level on affected beaches that have been eroding landward over the past three decades (Cooper et al., 2020; Pitman et al., 2024). The continued erosion of colliery spoil at the Co. Durham coastline has long been recognised as a source of PTEs (Giusti, 2001) with reported metal uptakes to marine algae and macroinvertebrates (Giusti, 2001; Giusti et al., 1999). However, the extent and nature of contaminant fluxes that occur during coal spoil erosion have never been fully characterised or quantified, meaning that the significance of these fluxes in comparison to other local PTE sources (e.g. riverine fluxes of metal(loid)s from industrial and mining sources) are unknown.

Therefore, this study seeks to investigate the mass fluxes of specific PTEs caused by the ongoing erosion of spoil terrace at these sites, and to characterise how erosion and seawater suspension alters the spoil composition, leaching behaviour and residual contamination risks. The specific objectives are: 1) to characterise the mineralogical and chemical composition of colliery spoils and related beach sediments present at affected beaches in Co. Durham; 2) to investigate spoil leaching behaviour as a function of pH and salinity; 3) to use coastal LiDAR survey data and aerial photography to estimate the volumes of spoil lost due to coastal erosion over the past two decades; and 4) use spoil composition and volume loss data to calculate element specific fluxes (with their associated uncertainties) in order to assess the importance of the impacts of coastal waste erosion relative to other pollution sources.

## 2. Methods and materials

### 2.1. Sample collection

Compacted colliery spoil samples and adjacent intertidal sediments were collected (Jan and Mar 2024) from 23 locations along the Co. Durham coastline previously affected by 20th century colliery spoil dumping (Fig. 1; SI Table S1). These sampling locations ensured that spoil and sediment samples were obtained from all known dumping sites on the Co Durham coastline and were also coincident with sites used by previous investigations (Alderton, 2012; Cooper et al., 2017; Gandy et al., 2025; Giusti, 2001). Blast beach and Horden beach were of particular focus as these were the locations of the most extensive disposals. At each location, 0.3-0.5 kg of colliery spoil was collected from exposed waste terraces (SI Figure S1) by combining six 50-100 g subsamples from approximately 10-20 m sections. Separate minimally disturbed spoil samples were also collected into sealed cylindrical plastic containers (polypropylene, length = 55 mm, ⌀ = 45 mm, volume = 70 ml) for moisture content and bulk density analysis. Where present, fine grained (<2 mm) intertidal sediments (0.5-1.0 kg) were collected from adjacent sand deposits located between the high and low tide levels. Each sample was a composite of ten 50-100 g subsamples of surface sediments (typically depth <2 cm, maximum 5 cm) from across a 10-20 $m^2$ area. All spoil and sediment samples were oven dried at 40 °C prior to gentle disaggregation in a mortar and pestle (where required) and homogenisation by mixing. Sub-samples of the bulk colliery spoil and the <2 mm fraction of intertidal sediments were then milled using a

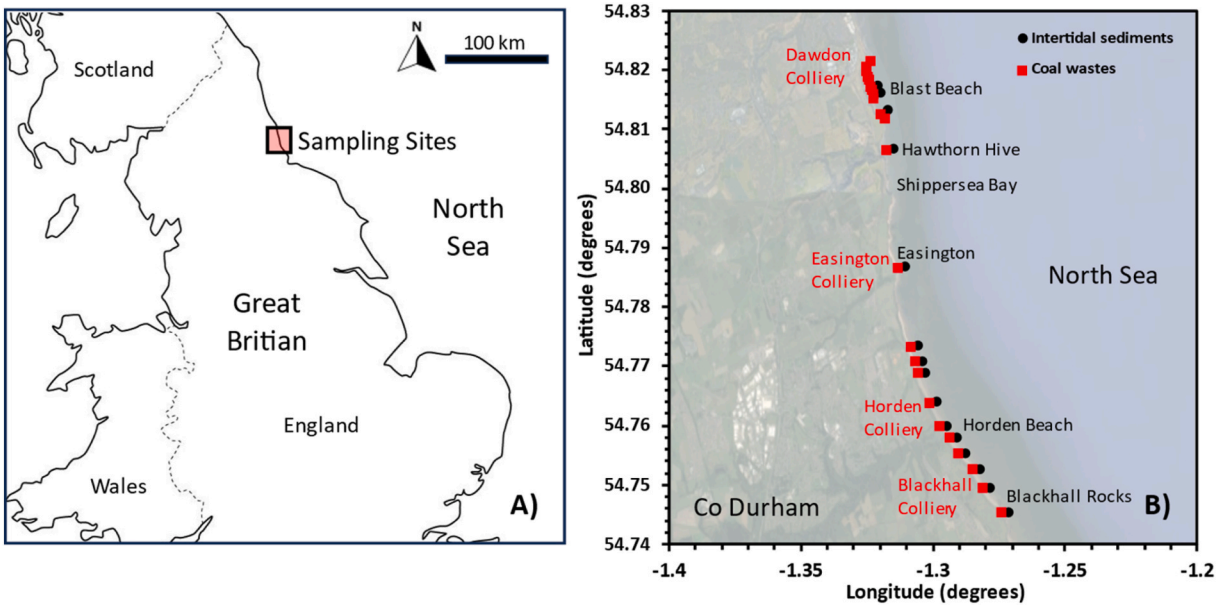


**Fig. 1.** A) location of the Co. Durham coastal colliery spoil sites in Northeast England; and B) Coal wastes and intertidal sediment sampling locations along with the four colliery locations where colliery spoil dumping occurred, and the coastal embayments and beaches containing compacted colliery spoil deposits.

Spex ball mill to produce powder samples for XRD and XRF analysis. Wet and dry weights were recorded for spoil samples collected in the 70 ml containers to allow calculation of in situ moisture content, bulk density, and dry bulk density.

### 2.2. Sample characterisation

Particle size distributions (PSDs) were obtained by dry sieving approximately 100 g samples using 2 mm, 180 μm and 63 μm sieves. Spoil samples used the dried materials from the 70 ml containers, therefore, had a maximum grainsize cut off at 45 mm (n.b. cobbles up to 30 cm were visible in the spoil during sampling). Intertidal sediments >2 mm were excluded from subsequent grainsize analyses. The >2 mm, 2 mm – 180 μm, 180 – 63 μm and <63 μm fractions from spoil samples, and the <180 μm fraction from sediment samples, were obtained for further analysis. The spoil samples contained an appreciable fine fraction. Therefore, selected <63 μm material was introduced as a dry powder to an X-Jet compressed air particle dispersion module (300 kPa) followed by grainsize determination by dynamic image analysis (25-30k images with 0.8-1.2 M particles per sample; lower limit of detection = 0.8 μm) using a Camsizer X2 dual camera particle analyser.

Powder X-ray diffraction (XRD) analysis was performed using Spex ball milled samples on a Bruker D8 diffractometer (50-100 mg powder samples mounted on silicon slides). Diffraction patterns were scanned from 2 to 86° 2θ for 1.1 h at a step size of 0.02° using a Cu tube operated at 40 kV and 40 mA. Relative phase abundance was assigned as follows: Major, Principal (100) Bragg reflection peak height was 51-100% of the largest peak present in the diffractogram; minor, principal peak height was 10-50% of largest peak; trace, principal peak height <10% of the largest peak. Milled powder samples were prepared as fused glass beads for major element analysis (1 g sample: 10 g 66% Li tetraborate/34% Li metaborate flux; fused at 1050 °C) or as pressed pellets for minor element analysis (6 g sample mixed with CEROX binder at a ratio of 4:1 then pressed to 10 ton in a 32 mm die). Elemental composition was then determined by X-ray fluorescence (XRF) on a Rigaku ZSX Primus II with an Rh tube. Total Hg concentrations were measured using a Lumex RA-915F Zeeman Hg Analyser and RAPID software. For the Hg analysis, powder samples were run in triplicate and certified reference material SRM 2710 (Montana I Soil certified by National Institute of Standards and Technology, USA) was used as a check standard during the analysis.

Colliery spoil and sediment samples (BB#4 and HP-BR#8) were prepared for scanning electron microscopy (SEM) analysis by embedding in epoxy resin blocks, which were then cut and polished using diamond pastes and water free lubricants to produce flat surfaces containing particle cross sections. After carbon coating (20 nm), back scattered electron images (BSEI) and elemental distribution maps were collected (working distance 15 mm; 20 keV) using a Tescan VEGA3 XM SEM equipped with an Oxford Instruments X-max 150 SDD Energy dispersive spectrometer (EDS) controlled by Aztec 3.3 software. Reflected light microscopy images were also collected from same blocks using a Leica DM750P polarising microscope fitted with a GXCAM Hichrome-HR4 digital camera.

Elemental and mineralogical data were not normally distributed (Shapiro Wilk, $P < 0.05$) therefore non parametric tests were used to analyse relationships between elements and key mineral phases (Spearman Rank) and to assess differences in concentrations of key elements between co-located spoil and fine intertidal sediment samples (Mann Whitney).

### 2.3. Leaching experiments

Colliery spoil collected from Blast Beach (20 g) was mixed with 200 ml natural seawater (SW) in a 500 ml conical flask (SI Figure S2), closed with a porous foam bung cap and placed on an orbital shaker (Stuart Scientific SSL1) at 150 rpm. This produced a mobile and aerated waste-water suspension designed to mimic waste interaction with seawater after erosion from waste terraces. A solid: solution ratio of 100 g L-1 was used for consistency with previous experiments on the same wastes (Gandy et al., 2025), which followed British Standard leaching test procedure BS EN 12457-2 (British Standards Institution, 2002). With reference to XRD and XRF data, samples typical for Co. Durham coastal spoils that were not compositional outliers were chosen for further analysis. Therefore, experiments were established in duplicate using samples from two locations (BB#1 and BB#4). Seawater was collected from Blast Beach in June 2024 (54.82169 °N, −1.32033 °E) and was filtered (0.45 μm; PES) prior to use in experiments. To maintain a 100 g $L^{-1}$ solid: solution ratio, each flask was weighed before and after sampling and water loss due to evaporation was replaced by addition of deionised water (DIW). At each sampling point, 10-15 ml waste-water suspension was withdrawn using a syringe and polypropylene tubing at selected intervals over 60 days. After sampling, the suspension was centrifuged (6000 *g*; 10 min) and the resultant supernatant was split into two fractions. The first fraction was used for pH and conductivity measurements using a Myron Ultrameter 6Psi. The second fraction was filtered (0.45 μm, PES) and retained for analysis by ICP-OES/MS. Seawater solutions were analysed on an Agilent 5800 Series ICP-OES or an Agilent 7700 Series ICP-MS as required.

In an additional set of tests, triplicate 4 g subsamples of Blast Beach colliery spoil (BB#4) were suspended in 40 ml solution in capped 50 ml polypropylene centrifuge tubes and shaken as above on an orbital shaker. These tests were designed to assess the effect of changing pH conditions on PTE leaching behaviour. The solutions used were either DIW, or 0.001, 0.1 or 0.1 mol $L^{-1}$ of $HNO_3$ or 0.001, 0.1 or 0.1 mol $L^{-1}$ NaOH, which equated to acid and base additions in the range of 0.01 – 1 mol $kg^{-1}$. After 7 days the tubes were centrifuged and the filtered (0.45 μm; PES) supernatant was analysed as above.

### 2.4. Temporal changes in colliery spoil volume and area

LiDAR (Light Detection And Ranging) topographic surveys were conducted along the Co. Durham coastline at 2 yearly intervals from 2010 to 2023 by the North East Regional Coastal Monitoring Programme, funded by the UK Environment Agency (Cooper et al., 2020). The derived topographic maps have a 1 m spatial resolution and therefore allow quantification of subaerial beach volume for the entire surveyed coastline, with typical vertical accuracies in the region of 0.05 - 0.15 m. Beach profiles were also measured twice per year (summer/-winter) between 2008 and 2023 using real time kinematic GNSS, with typical vertical accuracies of ±0.02 m. These surveys provide a continuous record of coastal change at these sites and allow the seasonal variability to be quantified in a way not possible from LiDAR data. The volume of unconsolidated sediment above current sea levels (0 m Ordnance Datum Newlyn; ODN) was calculated for each survey epoch in QGIS 3.22, and differencing between surveys allowed for the calculation of a time series of overall beach volumetric change. Volumetric change was also calculated for individual beach profile lines in the same manner. The area of Co. Durham beaches covered by colliery spoil was estimated by measurement of shapefiles produced for each embayment in Google Earth Pro v7.3.6.9285 for a series of aerial photography from 1985 to 2023. As the 1985 images were of low resolution, historical maps (UK Ordnance Survey) were used to confirm the position of the shoreline, which in 1985 was equivalent to the waste terrace extent at these sites (Pitman et al., 2024).

## 3. Results

### 3.1. Colliery spoil composition

Colliery spoil samples (Fig. 2a; <45 mm) were primarily composed of sand sized particles (63 μm-2 mm; 68 wt %), with small gravel (<2 mm; 16 wt %) and pelitic (15 wt%; <63 μm) fractions. Further separation of the <63 μm fraction revealed that 6.6 wt % (4.5-9.0 wt %)

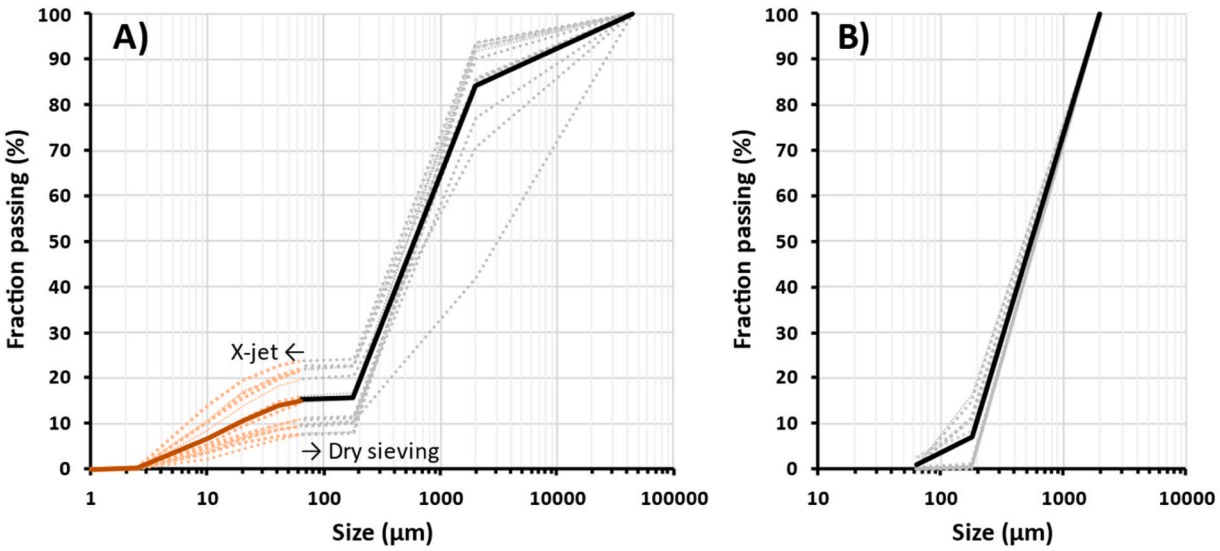


**Fig. 2.** Particle size distributions for; A) Compacted colliery spoil (<45 mm, n = 13) collected from Co Durham beaches and B) Intertidal sediments (<2 mm, n = 7) collected from adjacent locations. Solid line is the average value, and dashed lines are the individual measurements.

of the waste was present in the PM10 (particulate matter <10 μm) size fraction, but only 0.05 wt % and <0.002 wt % were present in the PM2.5 and PM1 size fractions, respectively. The median in-situ bulk density was 1.8 t $m^{-3}$ with a 21 wt % moisture content, producing a median dry bulk density of 1.4 t $m^{-3}$ (Table 1; SI Table S2). Quartz was a major or minor mineral present in all (n = 17) samples analysed (Fig. 3a; SI Figure S2). Other minerals such as kaolinite, muscovite, albite, microcline, chlorite, and hematite were also commonly present as minor or trace phases. Pyrite was present in a minority (4/17) of samples but was classified as a major phase in two samples. Jarosite or natrojarosite was detected in all samples (their primary peaks were not distinguishable by XRD). Gypsum was commonly (11/17) present, and barite and ankerite were also detected in some samples. $SiO_2$ (39 wt %) was the most common oxide detected, $Fe_2O_3$ (15 wt %) and $Al_2O_3$ (11 wt %) were also relatively abundant (Table 1). The spoil also had a relatively high loss on ignition value (23 wt %), consistent with high concentrations of hydrated minerals, or C and S containing phases. The spoil composition is relatively heterogenous (SI Table S3); $SiO_2$ and $Fe_2O_3$ concentrations are negatively correlated (i.e. high Si = low Fe; Spearman's $\rho = -0.48$, n = 17, p = <0.05), and $Fe_2O_3$ and total S content are positively correlated ($\rho = 0.76$, n = 17, p = <0.01). Total C is not correlated with $SiO_2$ ($\rho = 0.31$, n = 17, p = 0.23 but is negatively corelated with $Fe_2O_3$ ($\rho = -0.91$, n = 17, p = <0.01). This suggests the major compositional variance may be due to the relative proportions of Fe- and S- containing minerals to other phases present in each sample. In reflected light microscopy (SI Figure S3), 50-300 μm quartz and pyrite grains and coal fragments can be observed in the spoil (and considerable variation in the pyrite content between samples is apparent). Further analysis by SEM-EDS (Fig. 4a; SI Figure S5) shows pyrite, iron oxide, gypsum, and quartz grains within the spoil, and an abundant fine matrix phase containing a Fe-, S- and O, which is consistent with the jarosite minerals detected by XRD.

A wide range of potentially toxic element (PTEs) are present with the spoil (Table 1), many of which have median concentrations above background marine sediment concentrations (SI Table S4). A high percentage of samples contain As, Ba, Cr, Cu, Ni, Pb, Zn and Hg at concentrations above threshold sediment quality guidelines for ecosystem protection, and many samples contain As, Pb, Zn or Hg at concentrations above the probable effects levels (Persaud et al., 1993). Analysis of separated size fractions produced from colliery spoil samples (SI Figure S6) showed that mean Ba, Cu, V and Zn concentrations were not significantly different between the gravel (>2 mm), sand (<2 mm, >63 μm) or fine (<63 μm) fractions, and the bulk samples. As, Cr, Mo, Ni and Pb, however all have significantly higher mean concentrations in the <63 μm fractions.

### 3.2. Intertidal sediment composition

Intertidal sediments (n = 7; <2 mm) collected adjacent to the waste terraces were dominated (93 wt %) by medium/coarse sand sized particles (180 μm – 2 mm), with a minor (6 wt %) fine sand fraction (63 – 180 μm), with only 1 wt % present in the <63 μm fraction (Fig. 2b). Despite its relatively low wt. % abundance, the fine sand fraction (<180 μm) was selected for further chemical analysis as previous work (Giusti, 2001) found that the metal content in fine sand fraction was correlated with metal uptake by *Fucus vesiculosus* at these sites (and that the more commonly studied <63 μm pelitic, or 'mud', fraction was absent in these intertidal sediments). The <180 μm intertidal sediments contained a similar set of minerals to the colliery spoils (Fig. 3b). However, pyrite was detected in all samples (n = 5), but jarosite was present as a trace phase in only one sample (SI Figure S7). Calcite and dolomite were also both commonly present and siderite was detected in one sample. $Fe_2O_3$ (50 wt %) was the most common element detected, and $SiO_2$ (11 wt %) was the only other element with a median concentration >10 wt % (Table 1; SI Table S5). The sediments also had a high median loss on ignition value (27 wt %), consistent with high concentrations of pyrite-S. In microscopic analysis (SI Figure S4) the sediment samples were clearly related to adjacent coal wastes (i.e. the observed amount of pyrite in coal spoil was similar to the pyrite content of the adjacent sediments), however coal particles were much less abundant. The jarosite-rich fine fraction matrix was absent in some samples (Fig. 4b; SI Figure S3b), and pyrite and iron oxide particles appeared more rounded and had a O-rich, S-depleted altered surface layer consistent with both physical and chemical degradation. Significant deposits of similar Fe-rich sands were found at all the spoil affected sites (and are easily identifiable by their dark coloration; SI Figure S8). At these locations, Fe-rich sands commonly predominate the fine sediments in front of the spoil terraces, and in some locations, form unconsolidated deposits on top of the spoil (e.g. at Blast Beach).

As with the colliery spoil samples, a wide range of potentially toxic element (PTEs) were present in the <180 μm intertidal sediments (Table 1), which are also enriched compared background marine sediment concentrations (SI Table S6). A high % of samples contain As, Ba, Cr, Cu, Hg, Ni, Pb, and Zn at concentrations above threshold sediment

**Table 1**
Elemental composition, bulk density and in situ moisture content of colliery spoil and fine fraction (<180 μm) intertidal sediments. LOI = loss on ignition at 1050 °C; BD = in situ bulk density; DBD = dry bulk density; MC = moisture content; n.d. = not determined.

| | Units | Colliery spoil | | | Intertidal sediments | | |
|---|---|---|---|---|---|---|---|
| | | Median | *Min.* | *Max.* | Median | *Min.* | *Max.* |
| **$SiO_2$** | wt. % | 38.7 | *16.5* | *45.3* | 10.5 | *2.1* | *28.4* |
| **$TiO_2$** | wt. % | 0.5 | *0.1* | *0.8* | 0.2 | *0.2* | *0.4* |
| **$Al_2O_3$** | wt. % | 10.6 | *2.3* | *18.4* | 1.0 | *0.6* | *9.2* |
| **$Fe_2O_3$** | wt. % | 15.3 | *4.8* | *44.3* | 49.7 | *21.3* | *61.6* |
| **MnO** | wt. % | 0.0 | *0.0* | *0.1* | 0.1 | *0.1* | *0.1* |
| **MgO** | wt. % | 0.5 | *0.2* | *1.2* | 0.8 | *0.2* | *1.6* |
| **CaO** | wt. % | 0.6 | *0.2* | *4.5* | 2.5 | *0.2* | *8.2* |
| **$Na_2O$** | wt. % | 0.6 | *0.2* | *1.9* | 0.2 | *0.0* | *0.5* |
| **$K_2O$** | wt. % | 1.8 | *0.4* | *3.1* | 0.1 | *0.1* | *1.5* |
| **$P_2O_5$** | wt. % | 0.1 | *0.0* | *0.2* | 0.1 | *0.0* | *0.1* |
| **LOI** | wt. % | 23.0 | *18.5* | *40.0* | 26.6 | *23.0* | *29.6* |
| **XRF Total** | wt. % | 95.6 | *93.2* | *97.1* | 94.1 | *91.6* | *95.0* |
| **Total C** | wt. % | 4.6 | *1.1* | *21.1* | n.d. | *n.d.* | *n.d.* |
| **Total S** | wt. % | 4.3 | *0.7* | *35.2* | n.d. | *n.d.* | *n.d.* |
| **As** | mg $kg^{-1}$ | 122 | *47* | *509* | 159 | *120* | *184* |
| **Ba** | mg $kg^{-1}$ | 656 | *273* | *8440* | 2759 | *1060* | *9430* |
| **Co** | mg $kg^{-1}$ | 8 | *5* | *15* | 6 | *5* | *10* |
| **Cr** | mg $kg^{-1}$ | 56 | *25* | *113* | 75 | *17* | *124* |
| **Cu** | mg $kg^{-1}$ | 40 | *13* | *84* | 57 | *13* | *106* |
| **Mo** | mg $kg^{-1}$ | 24 | *9* | *79* | 23 | *18* | *30* |
| **Ni** | mg $kg^{-1}$ | 26 | *14* | *51* | 37 | *10* | *291* |
| **Pb** | mg $kg^{-1}$ | 86 | *32* | *664* | 55 | *29* | *475* |
| **V** | mg $kg^{-1}$ | 90 | *42* | *153* | 40 | *11* | *123* |
| **Zn** | mg $kg^{-1}$ | 84 | *23* | *336* | 384 | *113* | *1060* |
| **Hg** | mg $kg^{-1}$ | 0.50 | *0.24* | *1.22* | 1.87 | *0.88* | *2.13* |
| **BD** | t $m^{-3}$ | 1.8 | *1.2* | *2.0* | n.d. | *n.d.* | *n.d.* |
| **DBD** | t $m^{-3}$ | 1.4 | *1.1* | *1.7* | n.d. | *n.d.* | *n.d.* |
| **MC** | wt. % | 21 | *11* | *31* | n.d. | *n.d.* | *n.d.* |

quality guidelines, and many samples contain As, Hg or Zn at concentrations above the predicted effects levels (Persaud et al., 1993). Comparing concentrations of selected PTEs between colliery spoil and <180 μm intertidal sediments specific elements show contrasting trends. Median As, Cr and Cu concentration were not significantly different, V and Pb were significantly lower in sediments, and Hg and Zn were significantly higher (Fig. 5).

### 3.3. Elemental flux calculations

LiDAR survey data show that there was a significant loss of sediment volume within all the embayments containing colliery spoil deposits (Table 2). Detailed examination of the digital terrain models and beach profile transects produced from the LiDAR data (Fig. 6, SI figure S9) show that the material loss was overwhelmingly from erosion of the colliery spoil terraces. All six sites showed net volume losses between 2010 and 2023, with losses from the largest embayment, Horden, accounting for >80% of the total change. Examination of interannual variations in the loss rate within each embayment (Fig. 7a) shows that two periods of rapid mass loss (2012-2015 and 2017-2023) were interspersed with periods of small net gains that are associated with patterns of storm erosion and subsequent recovery in the unconsolidated beach sediments. The maximum waste area during the peak era of spoil disposal (1985, estimated from low resolution aerial photography and historical maps) was around 105 ha (Fig. 7b). Approximately half of this area was lost between 1985 and 2002, a period that included a major remedial intervention in addition to natural erosive losses (Cooper et al., 2017). After 2002, high resolution aerial photography allowed more accurate measurements of spoil covered areas present in each embayment. This showed that the rate of area loss slowed at every coastal unit except Horden. Linear extrapolation of the post 2002 area loss trends gave a minimum lifetime for the remaining spoil terraces of approximately 20 years; however, exponential extrapolation followed a decay function and suggests the spoil terrace may persist for >40 yrs.

The net volume change from 2010 to 2023 was combined with elemental concentration and dry bulk density data to produce a series of element specific annual flux estimates (Table 2). Flux estimates used the median elemental concentrations in colliery spoil and the median dry bulk density for the compacted wastes; quartile 1 (low) flux estimates used the lower quartile values for both elemental concentrations and dry bulk density; quartile 3 (high) flux estimates used the upper quartile values for both elemental concentrations and dry bulk density. Use of mean average elemental concentrations produced higher elemental fluxes, but these were still within the upper quartile 3 estimates (except for Ba where the mean value > upper quartile value). Detailed examination of the interannual variation elemental fluxes at Horden (SI Figure S10) show that annual variations in volume losses are the most important factor in determining elemental fluxes. The dry bulk density measures have a small interquartile range; therefore, density measurements are a low source of flux uncertainty. Based on median concentrations, As, V, Pb and Zn all have similar average annual fluxes at Horden between 2010 and 2023 (Table 2; 3.7-5.3 t $yr^{-1}$), however, very large differences in interquartile concentration ranges lead to differential uncertainty ranges. In particular, Pb had relatively low median spoil concentration (86 mg $kg^{-1}$) but also a significant number of high concentration samples (up to 664 mg $kg^{-1}$) producing much more uncertainty in the upper extent of possible Pb fluxes compared to As, V and Zn.

### 3.4. Leaching tests

Seven-day leaching tests using colliery spoil sample BB#4 and deionised water produced an acidic solution (pH 2.3; Table 3). A range of PTEs were also present in leachates, but the amounts leached were low compared to solid concentrations, with <1 wt % recovery for all elements tested, except for Cu, Ni and Zn (average of 1.2, 2.5 and 3.9 wt % recovery respectively). Leaching tests using progressively more acidic $HNO_3$ solutions produced progressively lower pH leachates and increasing amounts of PTEs recovered. The maximum recovery for all elements occurred at the highest $HNO_3$ addition (1.0 mol $kg^{-1}$) at pH < 1.5. Tests using alkaline solutions produced progressively higher pH values and lower PTE recoveries, with the lowest recoveries occurring in tests with 0.1 or 1.0 mol $kg^{-1}$ NaOH additions at pH 3.6 or 8.3. Many PTEs (Fe, As, Cr, Cu, Hg, Pb and V) displayed slightly amphoteric behaviour with slightly highly recoveries observed at pH 8.3 compared to pH 3.6. The 1.0 mol $kg^{-1}$ NaOH tests produced pH values close to seawater values (8.0-8.2 (Blackford and Gilbert, 2007);). To produce a similar base addition using BB#4 and just the alkalinity present in seawater (total alkalinity = 2.1-2.3 mmol $L^{-1}$ (Millero et al., 1998);) would require the spoil to be dispersed at a solution: solid ratio >450: 1 (i.e. approximately 2 g $L^{-1}$).

Two spoil samples from Blast Beach (BB#1 and BB#4) also produced acid solutions after suspension in seawater under aerobic conditions (Fig. 8). Although there was an initial difference in pH values between the two spoils, at the end of the test (60 days) pH values were very similar in the two experiments, and within the error margins of the pH probe (Table 4). Compared to the initial seawater samples prior to spoil

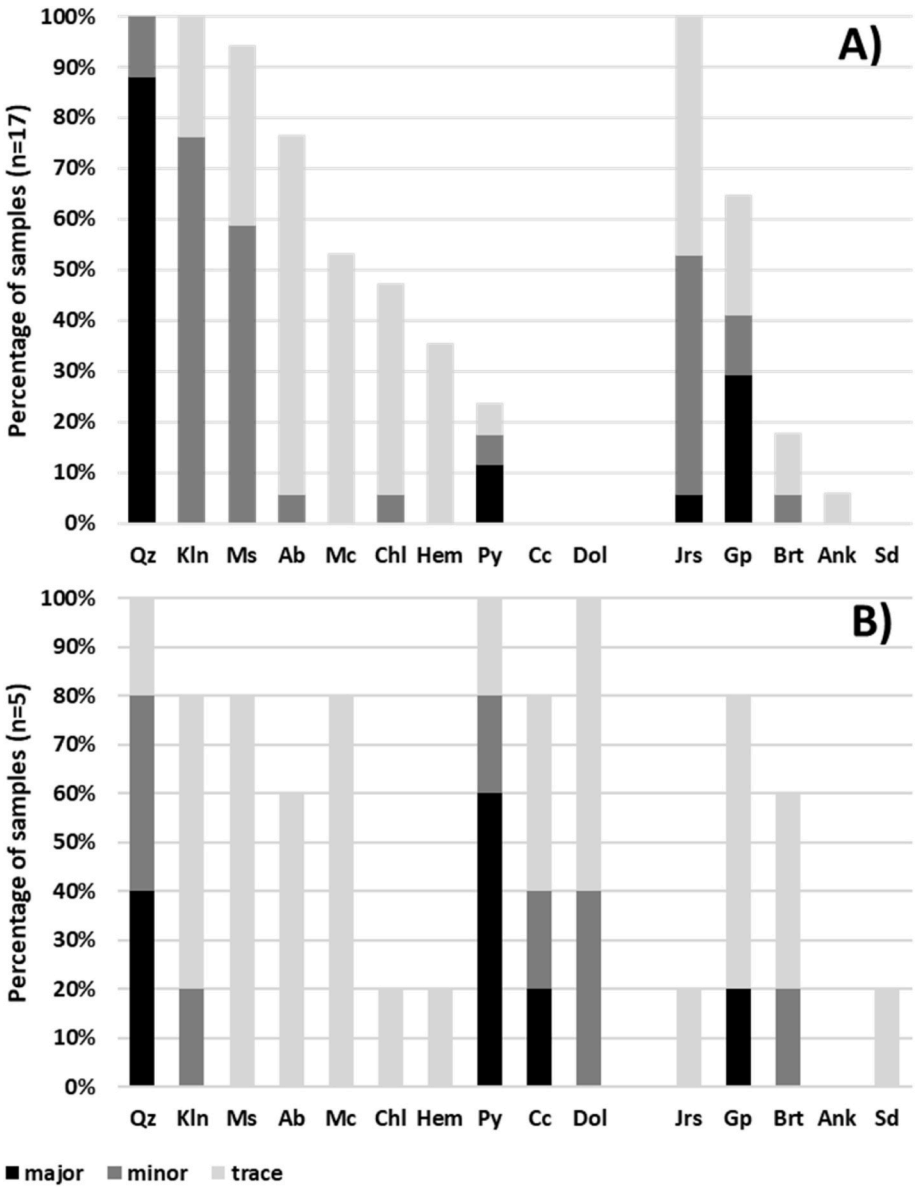


**Fig. 3.** Relative abundance of minerals detected in; A) Colliery spoil samples from Co Durham coastal sites, and B) < 180 μm intertidal sediments from adjacent locations. Key: Qz, quartz; Kln, kaolinite; Ms, muscovite; Ab, albite; Mc, microcline; Chl, chlorite; Hem, hematite; Py, pyrite; Cc, calcite; Dol, dolomite, Jrs, jarosite/natrojarosite; Gp, gypsum; Brt, barite; Ank, ankerite; Sd, siderite.

addition there was very little difference in concentrations observed for Na and Mg after 60 days. Calcium and S concentrations, however, were higher after 60 days (especially in the BB#1 experiments) and K concentrations were lower. Compared to seawater concentrations most of the measured trace elements (including, Ag, Al, As, Cd, Cr, Fe, Mn, Ni, Pb, Sb, and Zn) increased in concentration after 60 days. Only Co, Cu, and V concentration showed relatively little change compared to initial seawater concentrations. Experiments using sample BB#4 which had initially lower pH than the BB#1 experiments, also had initially higher concentrations of leached metal(loids) (Fig. 8). However, as the pH values converged over time, the differences in leaching behaviour also decreased over time.

## 4. Discussion

### 4.1. The effect of colliery spoil erosion on contaminant dispersion

The colliery spoil present at Co. Durham coastal sites was composed of a range of aluminosilicate minerals, coal fragments, pyrite and quartz grains consistent with its reported origin as the rejected material produced during coal washing (Eagle, 1979). When originally deposited, spoil at these sites was also reported to be a coarse-grained granular material with $D_{50} > 2$ mm (Eagle, 1979), and likely had a relatively low bulk density (1.0-1.2 t $m^{-3}$) similar to other fresh deposited colliery spoils (Burrows, 1982; Haigh et al., 2020; Kho and Williams, 2015). Since deposition, however, the spoil physically and chemically weathered in situ producing compacted spoil with much lower average grainsize ($D_{50} < 1$ mm), and higher bulk densities (1.2-2.0 t $m^{-3}$), similar to other compacted colliery spoil (Burrows, 1982; Haigh et al., 2020; Kho and Williams, 2015). The presence of higher proportions of fine particles, including secondary sulfate precipitates (e.g. gypsum, jarosite), often gave the compacted wastes a clay-like texture which is relatively cohesive, helping to form the waste terraces with near vertical faces observed at these sites (Fig. S1). The formation of jarosite (Equation (4)) also indicates that post depositional pyrite oxidation (Equations (1)–(3)) produced pH < 3 porewaters containing ferric sulfate ions

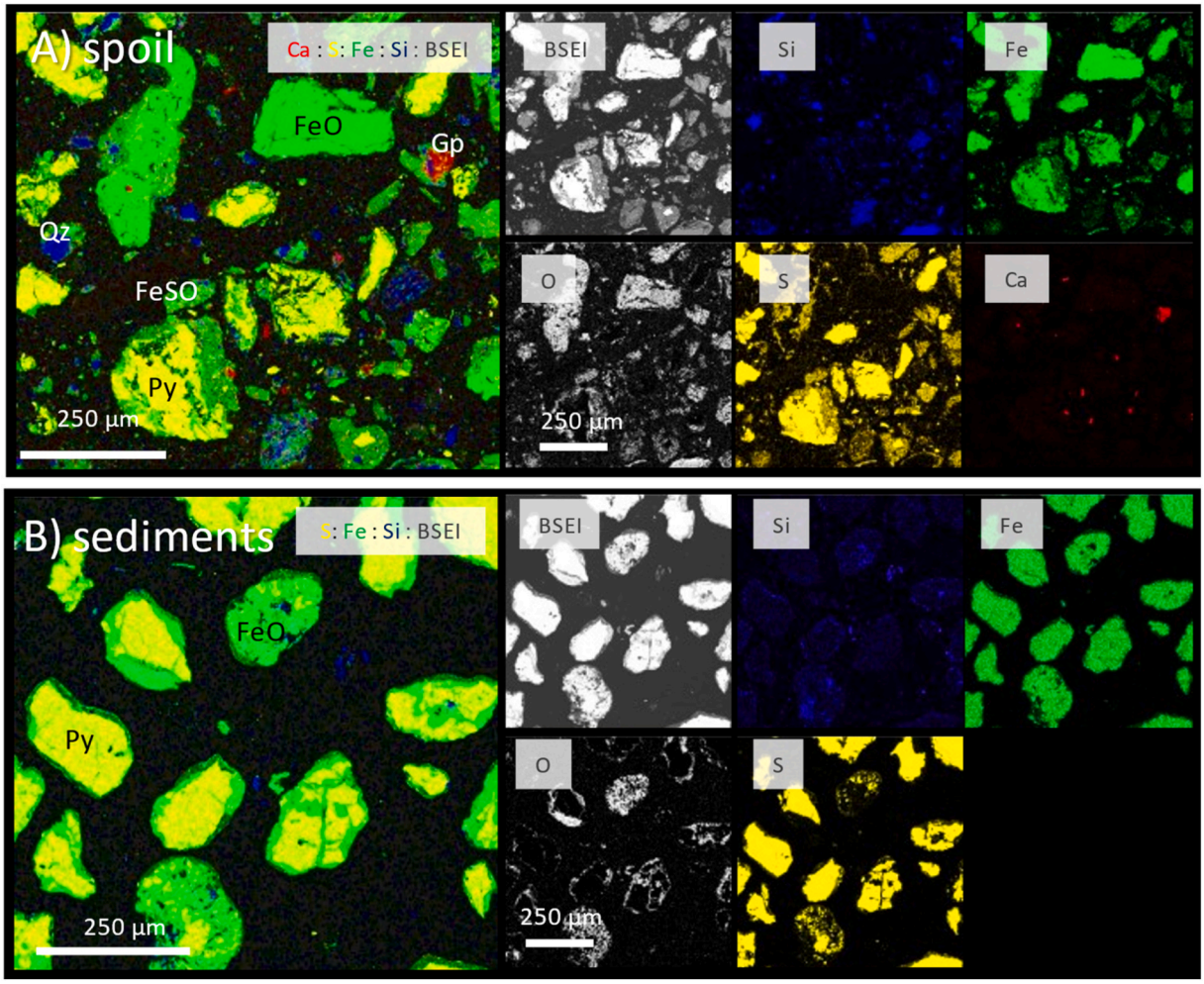


**Fig. 4.** False colour multi-element maps, BSE images and selected SEM-EDS elemental maps collected from A) Colliery spoil sample HP-BR #8, and B) intertidal sediments from an adjacent location. Key: Qz, quartz; Py, pyrite; Gp, gypsum; FeSO, iron sulfate phase; FeO, iron oxide phase. n.b. Ca was omitted from B) as no Ca was detected in the field of view shown. (For interpretation of the references to colour in this figure legend, the reader is referred to the Web version of this article.)

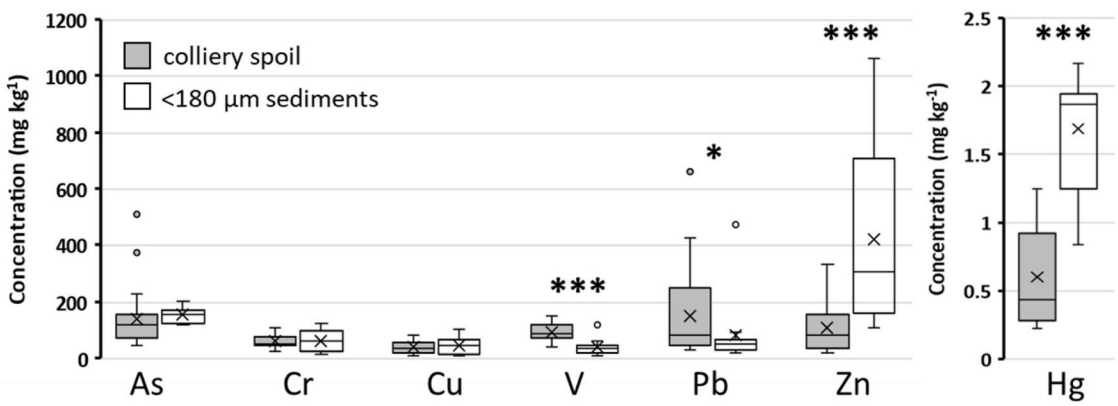


**Fig. 5.** Box and whisker plots showing selected elemental concentrations present in colliery spoil and adjacent <180 µm intertidal sediment samples collected from Co Durham beaches. Data sets marked with asterisks are different (spoil versus sediments) at the * 90%, ** 95% or *** 99% confidence level, respectively (Mann-Whitney *U* test).

(Smith et al., 2006) in an environment with a ready supply of monovalent cations ($K^+$, $Na^+$) from seawater.

$$(Na,K)^+ + 3Fe^{3+} + 2SO_4^{2-} + 6H_2O \rightarrow (Na,K)Fe_3(SO_4)_2(OH)_6 + 6H^+ \quad (4)$$

There was an apparent relationship between the spoil composition and the fine sand sediments found at adjacent locations (Fig. 4; SI Figure S4, S5) suggesting that spoil particles became incorporated in the beach sediments after erosion. However, the <63 µm fraction of the spoil was not retained in intertidal sediments and there was a distinct difference in the relative abundance of minerals present in the sediments

**Table 2**
Calculated element specific annual fluxes for selected potentially toxic elements caused by erosion of Co. Durham coastal colliery spoil deposits between 2010 and 2023. *Total combined 2022 annual releases to water from all industrial facilities listed in the UK Pollutant Release and Transfer Register (UK Government, 2025). #Metal mine discharges in England and Wales (Mayes et al., 2010).

| Embayment | Shoreline length | Volume change | Volume/ length | % losses | As | Ba | Co | Cr | Cu | Mo | Ni | Pb | V | Zn | Hg |
|---|---|---|---|---|---|---|---|---|---|---|---|---|---|---|---|
| units | m | $m^3$ | $m^3\ m^{-1}$ | % | t $yr^{-1}$ | t $yr^{-1}$ | t $yr^{-1}$ | t $yr^{-1}$ | t $yr^{-1}$ | t $yr^{-1}$ | t $yr^{-1}$ | t $yr^{-1}$ | t $yr^{-1}$ | t $yr^{-1}$ | t $yr^{-1}$ |
| Blast Beach | 1200 | −20946 | −17 | 4.2 | 0.28 | 1.48 | 0.02 | 0.13 | 0.09 | 0.05 | 0.06 | 0.19 | 0.20 | 0.19 | 0.0011 |
| Hawthorn Hive | 650 | −12746 | −20 | 2.5 | 0.17 | 0.90 | 0.01 | 0.08 | 0.05 | 0.03 | 0.04 | 0.12 | 0.12 | 0.12 | 0.0007 |
| Shippersea | 370 | −14881 | −40 | 3.0 | 0.20 | 1.05 | 0.01 | 0.09 | 0.06 | 0.04 | 0.04 | 0.14 | 0.14 | 0.13 | 0.0008 |
| Easington | 1420 | −12759 | −9 | 2.5 | 0.17 | 0.90 | 0.01 | 0.08 | 0.05 | 0.03 | 0.04 | 0.12 | 0.12 | 0.12 | 0.0007 |
| Horden | 4110 | −405466 | −99 | 80.9 | 5.33 | 28.6 | 0.35 | 2.45 | 1.75 | 1.05 | 1.14 | 3.76 | 3.93 | 3.67 | 0.0218 |
| Blackhall | 1400 | −34224 | −24 | 6.8 | 0.45 | 2.42 | 0.03 | 0.21 | 0.15 | 0.09 | 0.10 | 0.32 | 0.33 | 0.31 | 0.0018 |
| **TOTAL** | **9150** | **−501021** | **−55** | **100.0** | **6.58** | **35.4** | **0.43** | **3.02** | **2.16** | **1.29** | **1.40** | **4.64** | **4.86** | **4.53** | **0.027** |
| *Q1 estimate* | | | | | 4.00 | 18.0 | 0.36 | 2.50 | 1.20 | 0.60 | 1.00 | 2.50 | 3.90 | 1.90 | 0.016 |
| *Q3 estimate* | | | | | 9.00 | 50.1 | 0.52 | 3.40 | 3.40 | 2.10 | 2.10 | 14.60 | 7.00 | 9.00 | 0.057 |
| **Permitted Discharges 2022*** | | | | | **6.5** | | | **6.5** | **72.0** | | **35.7** | **11.0** | | **267** | **0.168** |
| **Metal Mine Discharges 2010#** | | | | | **5.1** | | | | **19.1** | | **2.1** | **18.5** | | **193** | |

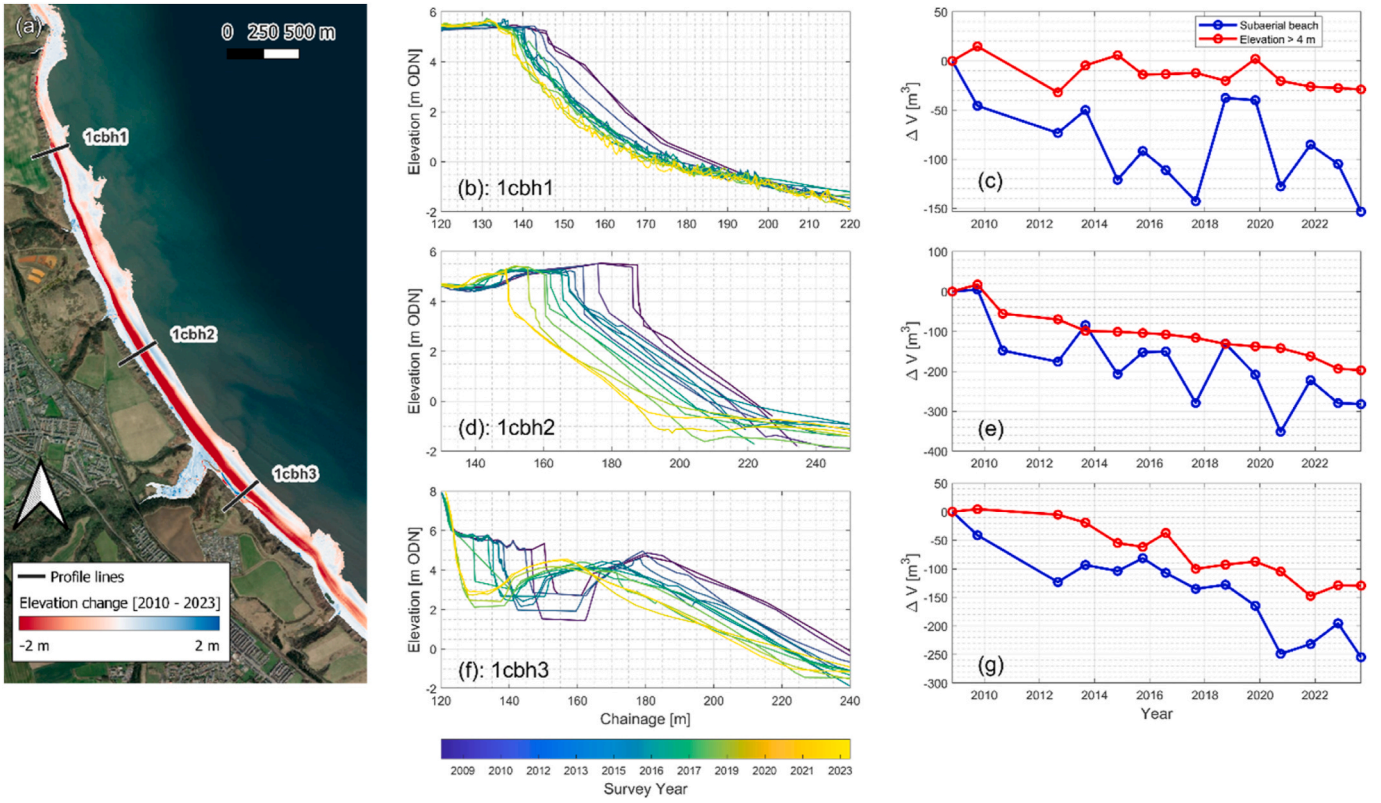


**Fig. 6.** A) LiDAR elevation map of Horden Beach, Co. Durham showing the total elevation change between 2010 and 2023 and individual beach profile changes (B, D, F) and beach volume changes (C, E, G) at the selected profiles shown in A). The blue line is indicative of volume changes for the entire subaerial beach (elevation >0 m ODN), whereas the red line shows only elevations more than 4 m which correlate to the upper elevations of the spoil terraces. (For interpretation of the references to colour in this figure legend, the reader is referred to the Web version of this article.)

compared to the spoil (Fig. 3). High density minerals (>5 g $cm^{-3}$; e.g. Fe-oxides, pyrite, barite) appear to have been preferentially retained relative to lower density minerals (<3 g $cm^{-3}$; e.g. quartz, feldspars, clays, coal, gypsum, jarosite). Therefore, winnowing and density separation of the eroded spoil created deposits of Fe-rich (~50 wt % as $Fe_2O_3$), pyrite-containing fine sands that contained higher concentrations of some potentially toxic elements (PTEs; e.g. As, Ba, Zn, Hg) than the spoil deposits from which they were derived; presumably as these elements were originally enriched in the high density retained particles. Other PTE concentrations (e.g. Pb, V) were lower in the fine sand sediments compared to spoil samples, presumably due to an original association with low density or fine-grained particles in the spoil, which are lost from the beaches due to winnowing of these particles. The preservation of carbonate minerals in the beach sediments in front of the spoil terraces (e.g. calcite, dolomite; derived from magnesium limestone cliffs) also indicates that, in contrast to the spoil deposits, pyrite oxidation did not produce acidic porewaters, most likely due to regular flushing with alkaline seawater.

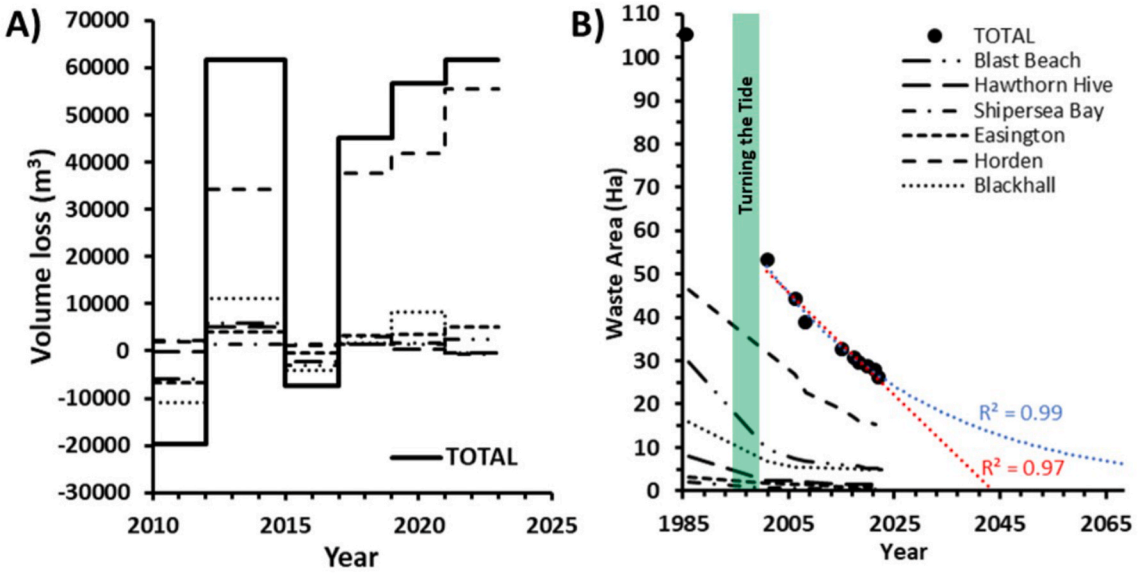


**Fig. 7.** Interannual variation in; A) mean beach volume loss from LiDAR survey data collected between 2010 and 2023 for the six embayments where colliery spoil was deposited at the Co. Durham coast and, B) area covered by colliery spoil from aerial photography (also informed by historical shoreline mapping) between 1985 and 2023.

**Table 3**
Effect of addition of different amounts of $HNO_3$ or NaOH on suspension pH and the leaching of selected elements from a colliery spoil sample from Blast Beach, Co. Durham (BB#4). Values are the mean of triplicate tests after 7 days; DIW = deionised water; ≤ less than the given limit of detection. Maximum values are in **bold** text; minimum values are in underlined text.

| Acid/base additions units | pH | Fe mg $kg^{-1}$ | Al mg $kg^{-1}$ | As mg $kg^{-1}$ | Cr mg $kg^{-1}$ | Co mg $kg^{-1}$ | Cu mg $kg^{-1}$ | Hg mg $kg^{-1}$ | Ni mg $kg^{-1}$ | Pb mg $kg^{-1}$ | V mg $kg^{-1}$ | Zn mg $kg^{-1}$ |
|---|---|---|---|---|---|---|---|---|---|---|---|---|
| $HNO_3$ 1.0 mol $kg^{-1}$ | <1.5 | **4230** | **151** | **0.86** | **0.38** | **0.17** | **1.31** | **0.0017** | **0.74** | **0.17** | **5.87** | **4.12** |
| $HNO_3$ 0.1 mol $kg^{-1}$ | 2.0 | 420 | 87.0 | 0.10 | 0.24 | 0.17 | 1.04 | <0.0003 | 0.69 | <0.004 | 0.39 | 3.96 |
| $HNO_3$ 0.01 mol $kg^{-1}$ | 2.3 | 226 | 72.2 | 0.09 | 0.20 | 0.16 | 0.59 | <0.0003 | 0.66 | 0.005 | 0.10 | 3.50 |
| DIW - | 2.3 | 157 | 64.7 | 0.06 | 0.18 | 0.16 | 0.51 | <0.0003 | 0.66 | 0.006 | 0.03 | 3.33 |
| NaOH 0.01 mol $kg^{-1}$ | 2.3 | 151 | 74.7 | 0.03 | 0.18 | 0.16 | 0.66 | <0.0003 | 0.67 | 0.006 | 0.02 | 3.69 |
| NaOH 0.1 mol $kg^{-1}$ | 3.6 | 2.30 | 9.60 | 0.02 | 0.01 | 0.08 | 0.01 | <0.0003 | 0.28 | <0.004 | 0.01 | 0.67 |
| NaOH 1.0 mol $kg^{-1}$ | **8.3** | 29.6 | 2.90 | 0.15 | 0.02 | 0.01 | 0.16 | 0.0012 | 0.04 | 0.007 | 0.02 | 0.04 |

Leaching tests can assess the potential aqueous release of PTEs both in situ and during seawater erosion. Scenarios involving either rainwater infiltration or seawater flooding are likely involved in waste being leached at high solid: solution ratios (the average moisture content of the spoil, 21 wt %, gives an approximate solid: solution ratio of 3800 g $L^{-1}$). In contrast, erosion and dispersion of the spoil into coastal waters will likely create suspensions with much lower solid: solution ratios. Contacting spoil samples with both DIW and seawater at 100 g $L^{-1}$ produced acidic solutions, most likely due to the rapid dissolution of jarosite (Equation (5)), which is a highly reactive acid sulfate salt (Welch et al., 2008).

$$KFe_3(SO_4)_2(OH)_6 + 3H_2O \rightarrow 3Fe(OH)_3 + K^+ + 2SO_4^{2-} + 3H^+ \quad (5)$$

Alternatively in low pH solutions, ferric hydroxides did not form, producing aqueous $Fe^{3+}$ ions that could have further catalysed pyrite oxidation (Equation (3)) to produce acidity. Relative to seawater concentrations there were also increases in Ca and S concentrations, likely due to dissolution of the gypsum present in the samples. As noted previously for similar spoil materials (Gandy et al., 2025), solution pH was the primary control on the amount of PTE release to solution (the lower the pH value the higher the concentrations of PTEs observed). In aerobic leaching experiments using a sample of Blast Beach spoil (BB#1), pH decreased from 3.9 to 3.2 over 60 days. There was also a reduction in K concentrations compared to seawater that likely indicated that jarosite formed during this period (Table 4). Therefore, we attribute the observed pH reduction to the slow oxidation of Fe(II) containing phases present in the spoil producing aqueous Fe(III), which in the presence of $K^+$ from seawater, promoted the formation of jarosite and generated acidity (Equation (4)). PTE concentrations in these specific experiments also increased as pH reduced (Fig. 8). For the metalloid As, this resulted in an apparent removal in the initial timepoints (up to 20 days) reversing to produce a net release in later timepoints (Fig. 8), highlighting the value of longer-term experiments in assessing PTE behaviour.

In leaching experiments in which spoil samples were contacted with NaOH, a 1.0 mol $kg^{-1}$ base addition was required to neutralise samples of Blast Beach spoil to pH 8.3, which is just above seawater values (and approximately equivalent to suspension of this spoil sample in seawater at 2 g $L^{-1}$). PTE release was also low at this pH value (≪ 1 % of the total PTEs present were solubilised) due to either the precipitation of metal (loid)s as oxyhydroxides or their sorption to mineral surfaces at

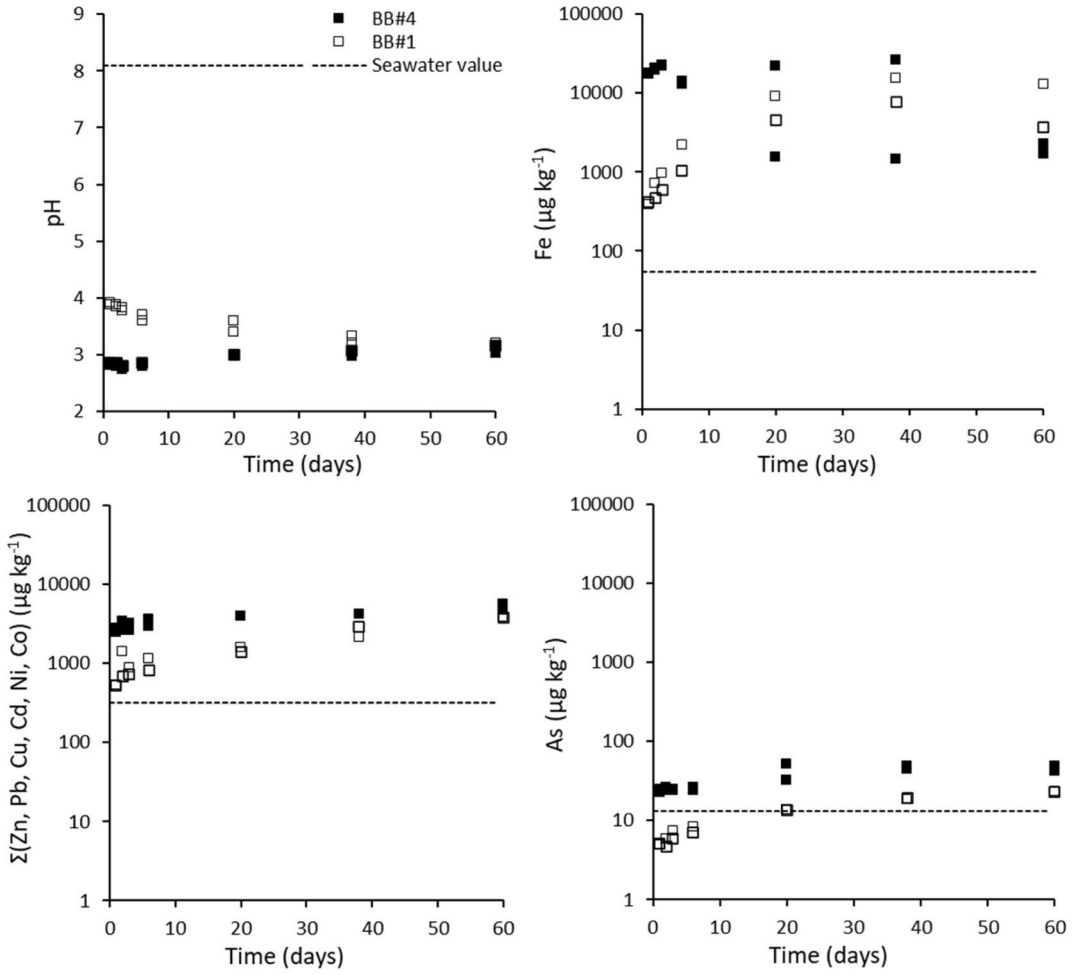


**Fig. 8.** Time dependant aerobic leaching behaviour of colliery spoil samples from Blast Beach (BB#1 and BB#4) after suspension in Co Durham coastal seawater.

circumneutral pH (Langmuir, 1997). Therefore, particulate fluxes, rather than dissolved metals, are likely to dominate PTE dispersion in the coastal environment following physical erosion of the spoil terraces.

### 4.2. Estimated element specific fluxes due to physical erosion

Calculation of element specific fluxes caused by spoil erosion requires a good understanding of the change in spoil terrace volumes, its dry bulk density, and its elemental composition. Available LiDAR data enabled the calculation of volume changes occurring at the Co. Durham coast from 2010 to 2023. Although there were some interannual variations in sediment volumes due to onshore movements of unconsolidated beach sediments in front of the spoil deposits, the dominant signal observed over longer timescales was the retreat of the colliery spoil terraces. Therefore, the total summed volume change observed between 2010 and 2023 (−501,021 $m^3$) was used to estimate the average annual spoil erosion rate. Analysis of aerial photography also revealed an area of spoil terrace totalling 12.8 ha (128,000 $m^2$) was lost during an overlapping period (2008-2022), equating to an approximate layer thickness of 3.9 m to give the volume loss detected from the LiDAR data. Although the exposed face of the spoil terraces rarely exceeded 2.5 m high, the elevation of the spoil terraces (4-6 m ODN) was sufficient to accommodate a 3.9 m spoil layer, and typically the lower sections of the wastes are covered by unconsolidated sediments. Indeed, following significant winter storms (e.g. following Storm Babet in October 2023) these unconsolidated beach sediments were removed, revealing that the spoil terraces were generally much deeper than the exposed sections (BBC online, 2023). Therefore, although it is a worst-case scenario to base flux calculations on the total observed volume change between 2010 and 2023 (i.e. that 100% of that material was colliery spoil), it is not an unreasonable assumption and is consistent with observations.

Although, there were variations in spoil composition between locations, (e.g. the average Ba concentration was higher at Blast Beach than other locations), it is impossible to know if the spoils currently exposed are representative of materials previously eroded prior to sampling. Therefore, it was assumed that the sampled spoil was broadly representative of the eroded material in this region, and the median dry bulk density measurements and median elemental concentrations from all sampled locations were used in flux calculations (with their interquartile ranges used to produce high and low flux estimates, respectively).

This was achieved in two steps. Firstly, the annualised rate of volume loss was converted to an annualised mass loss using median dry bulk density measurements (Equation (6));

$$\text{Mass Loss (kg yr}^{-1}) = \text{Volume Loss (m3 yr}^{-1}) \text{ x Dry Bulk Density (kg m}^{-3}), \quad (6)$$

which in turn, was used to estimate the element specific fluxes using the median spoil elemental composition (Equation (7)),

$$\text{Elemental Flux (mg yr}^{-1}) = \text{Mass Loss (kg yr}^{-1}) \text{ x Concentration (mg kg}^{-1}), \quad (7)$$

Finaly, the elemental fluxes were converted to t $yr^{-1}$ to allow comparison to other flux data sets. Given the uncertainties involved, the resultant average elemental fluxes for the 2010-2023 period can only be treated as estimates. However, these PTE fluxes provide insights on the

**Table 4**
Comparison of solution composition for selected elements in long term aerobic seawater leaching experiments using colliery spoil samples from Blast Beach Co. Durham (BB#1; BB#4; 60 days; 100 g $L^{-1}$ suspension; mean ± range of duplicates) and the initial seawater samples collected from the same location.

| | Units | BB#1 | BB#4 | Seawater |
|---|---|---|---|---|
| pH | - | 3.2 ± 0.0 | 3.1 ± 0.1 | 8.1 ± 0.0 |
| **Conductivity** | mS $cm^{-1}$ | 73.9 ± 1.0 | 71.4 ± 0.6 | 47.9 ± 0.6 |
| *Major Elements* | | | | |
| **Ca** | mg $L^{-1}$ | 1100 ± 100 | 340 ± 1 | 377 ± 50 |
| **Mg** | mg $L^{-1}$ | 1040 ± 130 | 990 ± 3 | 1140 ± 160 |
| **Na** | mg $L^{-1}$ | 8710 ± 930 | 8270 ± 40 | 9130 ± 190 |
| **K** | mg $L^{-1}$ | 360 ± 90 | 280 ± 10 | 490 ± 60 |
| **S** | mg $L^{-1}$ | 1560 ± 60 | 880 ± 10 | 790 ± 14 |
| **Si** | mg $L^{-1}$ | 68 ± 4.4 | 61 ± 1.1 | 0.5 ± 0.0 |
| *Trace Elements* | | | | |
| **Ag** | µg $L^{-1}$ | 4.3 ± 0.6 | 5.1 ± 0.1 | 0.3 ± 0.1 |
| **Al** | µg $L^{-1}$ | 3510 ± 590 | 8060 ± 620 | 10 ± 0.0 |
| **As** | µg $L^{-1}$ | 2.3 ± 0.0 | 4.5 ± 0.1 | 1.3 ± 0.1 |
| **Cd** | µg $L^{-1}$ | 1.1 ± 0.2 | 4.6 ± 0.5 | <0.1 |
| **Co** | µg $L^{-1}$ | 15 ± 1.0 | 29 ± 1.5 | 13 ± 0.3 |
| **Cu** | µg $L^{-1}$ | 12 ± 1 | 9 ± 2 | 13 ± 0.3 |
| **Cr** | µg $L^{-1}$ | 2.4 ± 0.1 | 3.9 ± 0.6 | 0.2 ± 0.1 |
| **Fe** | µg $L^{-1}$ | 831 ± 651 | 196 ± 40 | 5.4 ± 0.1 |
| **Hg** | µg $L^{-1}$ | <0.1 | <0.1 | <0.1 |
| **Mn** | µg $L^{-1}$ | 160 ± 10 | 450 ± 40 | 1.5 ± 0.0 |
| **Ni** | µg $L^{-1}$ | 61 ± 1.5 | 110 ± 10 | 2.3 ± 0.3 |
| **Pb** | µg $L^{-1}$ | 3.7 ± 1.0 | 7.4 ± 1.4 | <0.1 |
| **Sb** | µg $L^{-1}$ | 7.4 ± 5.9 | 9.0 ± 8.4 | 0.3 ± 0.0 |
| **V** | µg $L^{-1}$ | 0.3 ± 0.0 | 0.4 ± 0.0 | 1.2 ± 0.1 |
| **Zn** | µg $L^{-1}$ | 290 ± 3 | 360 ± 60 | 3.6 ± 3.4 |

scale and timing of releases that have occurred at these sites and highlight the regional significance of colliery spoil deposits as a pollution source relative to other potential sources. Mayes et al. (2010) estimated that abandoned metal mine water discharges were by far the single biggest source of metals (e.g. Cd, Pb, Zn) to the freshwaters of England and Wales. The other major source for which data exist is UK industrial discharges (UK Government (2025). Whist the environmental setting is different (i.e. discharges to freshwaters, primarily of dissolved metals in the case of mine waters), both mine waters and industrial discharges ultimately discharge to marine environments, and therefore a comparison of metal(loid) fluxes from these sources with fluxes from coastal mine wastes provides some context for the observed fluxes in this study. Compared to total permitted UK industrial discharges (UK Government, 2025) and estimated total metal mine discharges in England and Wales (Mayes et al., 2010), the estimated annual fluxes of metal(loids) due to spoil erosion are generally lower (except for As) but are certainly not trivial (Table 2). The calculated fluxes of As, Cr, Hg and Pb, highlight that erosion of the colliery spoil terraces may be a significant source of these elements to the North Sea. Indeed, the total recorded 2022 permitted PTE discharges (for As, Cr, Cu, Pb, Hg, Ni and Zn) in the Northumbria River Basin District (which contains the Co. Durham colliery spoil sites) was 12.0 t $a^{-1}$ (from 12 facilities), which compares to the estimated flux of 22.3 (13.1 – 41.6) t $a^{-1}$ for the same PTEs released by colliery spoil erosion between 2010 and 2023. The high As flux is of particular concern as there are no other significant local sources of As, either from inland mine discharges (Mayes et al., 2010), or from permitted discharges. During the 2010-2023 period, there was also observed interannual variation in fluxes, with two periods with above average erosion, balanced by two quiescent periods with little or no erosion recorded (Fig. S10). Therefore, the episodic nature of the erosive fluxes may pose a greater risk to adjacent marine ecosystems than from other more diffuse sources. Interannual variations in coastal erosion at these sites are driven by the occurrence of intense winter storm events (Pitman et al., 2024). North Atlantic storm intensities have multiple climatic influences including an observed relationship to the El Nino Southern Oscillation (ENSO), where storm formation is reduced following warm El Nino events, and enhanced after colder La Nina events (Keim et al., 2004). Global warming is expected to amplify ENSO events (Latif and Keenlyside, 2009), however, how this may impact on North Atlantic storm intensities and UK coastal erosion rates is not yet understood.

### 4.3. Implications for spread of contaminants and coastal management

Although the present day colliery spoil terraces are important sources of PTEs to the coastal environment, it should be noted that the estimated annual PTE fluxes for the 2010-2023 period are likely to be significantly lower than historical fluxes occurring during the 20th century when active spoil dumping occurred at Dawdon, Easington, Horden, and Blackhall collieries (approximately 1900-1990s), and the period immediately after the cessation of tipping when shorelines were around 200 m seaward of their current positions (Cooper et al., 2017). Analysis of aerial photographs revealed that 26.1 ha of beaches were covered in spoil in March 2022. Assuming a 3.9 m layer thickness (see section 4.2 above) this equates to approximately 1.0 million $m^3$ of spoil. Therefore >95 % of the originally tipped spoil (39 million $m^3$; Pitman et al., 2024) has already been transported offshore. This will have produced high inventories of PTEs in affected marine sediments and may constitute a long-term environmental hazard to North Sea ecosystems (e.g. if remobilised during intense storm events, sea bottom trawling, installation of offshore energy infrastructure, or cutting trenches for associated cables), even if all the remaining onshore spoil deposits were immediately removed. Previous workers (Rowlatt and Lovell, 1994) have found significant PTE anomalies (for Cr, Pb, and Zn) in marine sediments adjacent to the spoil dumping sites although a definite link to spoil dumping has not yet been established and should be the focus of future investigation.

Even though most of the disposed spoil has been transported offshore, a Fe-rich pyrite-containing fine sand fraction has been retained in the nearshore environment; this is far from a benign material and may constitute the main vector of contaminant spread into shoreline ecosystems as these high-density particles will be better retained in high energy environments (e.g. rocky shore environments) than lower density particles, and the pyrite component will further oxidise over time releasing any associated PTEs. Previous work has suggested a clear relationship between the fine sand PTE concentrations and PTE concentrations in marine organisms at these sites. Giusti et al. (1999) identified elevated concentrations of several PTEs (Fe, Mn, Zn, Cr, Cu, Pb, Ni, Cd and Ag) in mussels (*Mytilus edulis*) at the same sites as investigated here, and Giusti (2001) also identified significant correlations between PTE concentrations in intertidal sediments and the brown alga *Fucus vesiculosus*, also at the same sites and for the same metals as reported in Giusti et al. (1999). More recently, elevated concentrations of PTEs in intertidal zone biota (the limpet *Patella vulgata* and *Fucus* spp.) were measured adjacent to metal-bearing legacy landfill material deposited by a landslide onto a beach in southern England (Pope et al., 2011). These lines of evidence suggest that at least a proportion of the elevated PTEs in intertidal sediments at these sites may also be bioavailable, though contemporary direct determinations would be a useful addition to the research reported here.

The rate of decrease in beach area covered by spoil since 2001 can be fit equally well by both linear ($R^2 = 0.97$) or exponential ($R^2 = 0.99$) regression. Projecting these mathematical fits into the future implies quite different outcomes in terms of spoil terrace longevity. A linear projection implies that the rate of area loss experienced since 2001 will remain constant into the future and complete removal of all remaining spoil would be expected before 2045 (Fig. 7b). However, this does not consider if the remaining spoil deposits will be preserved in progressively more protected areas at the back of beaches, causing the rate of erosion to slow (matching the exponential curve). The rate of area loss has, in fact, slowed at some of the locations containing spoil deposits. Separate linear projections for the individual embayments, predict that

at the current rate of removal, spoil will still be present at Blast Beach and Blackhall for more than 30 years. In contrast, Horden Beach is bigger, much more open, and not protected by headlands; at the current removal rate the spoil terraces at this site will be gone in just over 10 years. Future climate related changes (including higher sea levels and increased storm activity) may also increase the rate of colliery spoil erosion at these sites by exposing protected backshore areas to wave action, further reducing their expected longevity (Burningham and French, 2017; Robins et al., 2016; Toimil et al., 2020).

Pitman et al. (2024) highlighted that the presence of colliery spoil terraces at these sites have interrupted natural coastal erosion processes, especially by protecting the limestone cliffs present at the back of these embayments (which have not faced the full force of the sea in over 100 years, Fig. S11). As a result, rather than being actively eroded by the sea, these cliffs have weathered in situ, with no waves to remove loose sediment or break apart weaker sections. This prolonged period of relative stability means that, if the spoil terraces are eventually eroded away, the cliffs could undergo a phase of rapid adjustment—often referred to as 'coastal catchup'—as they respond to renewed wave exposure (Dornbusch and Mylroie, 2018; Walkden et al., 2016). Given that the spoil terraces may be removed by erosion in the next few decades, coastal managers should now be considering the impacts that reactivated cliff erosion may have on local infrastructure (e.g. the railway viaduct present at Hawthorn Hive) and public access.

It should also be noted that all the colliery spoil terraces in the Co. Durham area are located on beaches with unrestricted public access and are generally well used recreational areas. Therefore, there may be risks to beach users with respect to contact with the spoil, the associated acidic ponds, or exposure to waste derived dust emissions. Therefore, further work is required to assess if the wastes present on these beaches pose a risk to human health via, inhalation, dermal or ingestion pathways, and how any specific risks compare to other common environmental risks (Tainio et al., 2016).

### 4.4. *Wider implications for management of coastal waste sites*

The overall environmental impact of pollution fluxes from legacy waste sites on coastal ecosystems needs to be assessed within a regional context. In the past several decades access to high resolution aerial photography and beach survey data (especially regular LiDAR profiling) has provided a great opportunity to understand recent changes in coastline position and volume changes (Pitman et al., 2024). Where suitable databases of waste deposits are also available (Riley et al., 2022), this volume change information can be combined with physical and chemical compositional data to estimate annual fluxes of specific contaminants, with appropriate uncertainties and a basic understanding of interannual variability. Flux estimates can be compared with other permitted and non-permitted inputs to the coastal environment to assess the relative importance of legacy waste deposits. A key future uncertainty surrounds the extrapolation of recent erosion rates in the context of increased erosion expectations due to climate change (Environment Agency, 2024). Another key challenge is that for many sites, waste composition information is often absent or insufficient in national databases. For more important sites, detailed geochemical investigations are appropriate, but for smaller more widely dispersed deposits, good quality compositional databases are also required so that data from well-characterised sites can be better extrapolated to the majority of sites.

In general leachate fluxes from a range of coastal wastes are relatively low (Brand and Spencer, 2020; Gandy et al., 2025; Riley et al., 2024), but may be important while individual waste deposits remain intact. However, once waste deposits have been breached, particulate fluxes will likely dominate (and continued inclusion of leachate fluxes in calculations may result in double counting). Post deposition weathering reactions and erosion processes must also be considered. In the specific case of colliery spoil, weathering causes significant changes in the mineral composition and redistribution of PTEs as a function of grainsize. During erosion this can lead to preferential loss (or retention) of PTEs from nearshore locations, and the ratio of PTEs in affected marine sediments may not directly reflect the waste sources present. Finally, the work presented here again underlines the unsuitability of marine disposal options for mining wastes, especially in nearshore locations.

## 5. Conclusions

Colliery spoil terraces present on Co. Durham beaches for over 100 years contain concentrations of potentially toxic elements (PTEs, e.g. As, Pb, Zn and Hg) that may cause detrimental ecosystem effects when mobilised in coastal environments. Winnowing and density sorting during erosion caused the preferential retention of Fe-oxide and pyrite grains in intertidal fine sand sediments, which can contain higher concentrations of some PTEs (e.g. Ba, Hg and Zn) than the parent materials. Annual flux estimates indicate that spoil erosion has been a significant local source of several PTEs (including As, Cr, Hg, Pb and Zn) over the past two decades, and that these fluxes have been episodic in nature responding to pulses of coastal erosion. The high arsenic fluxes from spoil deposits are of particular concern due to the lack of other significant sources of this element to local marine environments. Three decades after the cessation of tipping, less than 5% of the originally tipped spoil is now retained on beaches, indicating that widespread contamination of adjacent marine sediments is likely to have already occurred. Overall, this work shows that erosion of coast legacy wastes remains a significant pollution source to coastal ecosystems (the remaining spoil at these sites are predicted to be eroded over multi-decadal timescales) which may increase in future due to accelerated erosion due climate induced sea level rises.

## CRediT authorship contribution statement

**Ian T. Burke:** Conceptualization, Data curation, Formal analysis, Funding acquisition, Investigation, Methodology, Project administration, Supervision, Writing – original draft, Writing – review & editing. **Sebastian J. Pitman:** Conceptualization, Data curation, Formal analysis, Funding acquisition, Investigation, Methodology, Writing – original draft, Writing – review & editing. **James Hodson:** Formal analysis, Investigation, Methodology, Writing – review & editing. **Lin Niu:** Data curation, Formal analysis, Investigation. **Fatmah Mohammed:** Data curation, Formal analysis, Investigation, Methodology. **Jenni Ilari Skakunova:** Formal analysis, Investigation. **Alex L. Riley:** Conceptualization, Funding acquisition, Investigation, Methodology, Writing – review & editing. **Catherine J. Gandy:** Formal analysis, Funding acquisition, Methodology. **Elliot Whitehead:** Formal analysis, Investigation, Methodology. **Karen A. Hudson-Edwards:** Formal analysis, Funding acquisition, Methodology, Supervision, Writing – original draft, Writing – review & editing. **Elin Jennings:** Formal analysis, Investigation, Methodology. **Helen Jay:** Conceptualization, Writing – review & editing. **Nick Cooper:** Conceptualization, Funding acquisition, Writing – review & editing. **Adam P. Jarvis:** Conceptualization, Data curation, Formal analysis, Funding acquisition, Investigation, Methodology, Project administration, Supervision, Writing – original draft, Writing – review & editing. **William M. Mayes:** Conceptualization, Funding acquisition, Investigation, Methodology, Supervision, Writing – original draft, Writing – review & editing.

## Declaration of competing interest

The authors declare the following financial interests/personal relationships which may be considered as potential competing interests: Ian Burke reports financial support was provided by UK Research and Innovation Natural Environment Research Council. Sebastian Pitman reports financial support was provided by British Society For Geomorphology. If there are other authors, they declare that they have no

known competing financial interests or personal relationships that could have appeared to influence the work reported in this paper.

## 7. Acknowledgements

This work was funded by the Natural Environment Research Council under grant numbers NE/T003022/1 (Legacy wastes in the coastal zone: Environmental risks and management futures); and NE/Y006518/1 (StormFlux: Effect of Storm Babet on pollution fluxes from remobilised mine wastes), and by the British Society for Geomorphology under grant number BSG-2021-07. We also acknowledge help from Lesley Neve, Richard Walshaw, Helena Brown, Stephen Reid, Jared West and Douglas Stewart (all University of Leeds), and access to the following University of Leeds facilities; Cohen geochemistry, Sediment, soil and pollutant analysis, Aqueous analysis, Leeds electron microscopy and spectroscopy, and X-ray diffraction and fluorescence.

## Appendix A. Supplementary data

Supplementary data to this article can be found online at https://doi.org/10.1016/j.apgeochem.2026.106899.

## Data availability

Data will be made available on request.

## References

Acharya, B.S., Kharel, G., 2020. Acid mine drainage from coal mining in the united States–An overview. J. Hydrol. 588, 125061.
Alderton, S., 2012. *Heavy Metal Contamination Along the Coast of North-East England* Durham University].
BBC online, 2023. Durham coastline: concern storm babet will escalate cliff erosion. BBC news. https://www.bbc.co.uk/news/uk-england-tyne-67193652.
Blackford, J., Gilbert, F., 2007. pH variability and CO2 induced acidification in the north sea. J. Mar. Syst. 64 (1–4), 229–241.
Brand, J.H., Spencer, K.L., 2020. Will flooding or erosion of historic landfills result in a significant release of soluble contaminants to the coastal zone? Sci. Total Environ. 724, 138150. https://doi.org/10.1016/j.scitotenv.2020.138150.
British Standards Institution, 2002. BS EN 12457–2:2002 Characterisation of Waste - Leaching – Compliance Test for Leaching of Granular Waste Materials and Sludges – Part 2: One Part Batch Test at a Liquid to Solid Ratio of 10 L/Kg for Materials with Particle Size Below 4 Mm (Without or with Size Reduction). British Standards Institution, London.
Brunskill, G.J., 2012. Mine waste disposal in the ocean an introduction. Oceanography (Wash. D. C.) 25 (2), 166–169. http://www.jstor.org/stable/24861354.
Burningham, H., French, J., 2017. Understanding coastal change using shoreline trend analysis supported by cluster-based segmentation. Geomorphology 282, 131–149.
Burrows, F., 1982. Root growth of clover on compacted colliery spoil. Miner. Environ. 4, 156–158.
Chugh, Y.P., Behum, P.T., 2014. Coal waste management practices in the USA: an overview. Int. J. Coal Sci. Technol. 1, 163–176.
Cooper, N., Benson, N., McNeill, A., Siddle, R., 2017. Changing coastlines in NE England: a legacy of colliery spoil tipping and the effects of its cessation. Proc. Yorks. Geol. Soc. 61 (3), 217–229.
Cooper, N., Siddle, R., Rowe, S., 2020. The value of monitoring data to sustainable coastal management in northeast England. In: Coastal Management 2019: Joining Forces to Shape our Future Coasts. ICE Publishing, pp. 185–199.
Dold, B., 2014. Submarine tailings disposal (STD)—A review. Minerals 4 (3), 642–666.
Dornbusch, U., Mylroie, P., 2018. Examples of coastal catch-up including barrier roll-back, marsh and brick-earth cliff erosion in southeast England. In: Coasts, Marine Structures and Breakwaters 2017: Realising the Potential. ICE Publishing, pp. 83–92.
Eagle, R., 1979. The field assessment of dumping wastes at sea. In: The Disposal of Solid Wastes off the north-east Coast of England, vol. 5.
Edinger, E., 2012. Gold Mining and Submarine Tailings Disposal Review and Case Study. Oceanography 25 (2), 184–199. http://www.jstor.org/stable/24861356.
Environment Agency, 2024. National assessment of flood and coastal erosion risk in England 2024. Gov.uk Retrieved from. https://www.gov.uk/government/publications/national-assessment-of-flood-and-coastal-erosion-risk-in-england-2024/national-assessment-of-flood-and-coastal-erosion-risk-in-england-2024.
Gandy, C.J., Burke, I.T., Byrne, P., Cooper, N., Crane, R.A., Hudson-Edwards, K.A., Mayes, W.M., Onnis, P., Riley, A.L., Jarvis, A.P., 2025. Spatial variability of metal (Loid) leaching from coastal colliery wastes under freshwater and saline water conditions. J. Environ. Manag. 376 (12448), 9.
Giusti, L., 2001. Heavy metal contamination of brown seaweed and sediments from the UK coastline between the wear river and the tees river. Environ. Int. 26 (4), 275–286.
Giusti, L., Williamson, A., Mistry, A., 1999. Biologically available trace metals in Mytilus edulis from the Coast of northeast England. Environ. Int. 25 (8), 969–981.
Haigh, M., Woodruffe, P., D'Aucourt, M., Alun, E., Wilding, G., Fitzpatrick, S., Filcheva, E., Noustorova, M., 2020. Successful ecological regeneration of opencast coal mine spoils through forestation: from cradle to grove. Minerals 10 (5), 461.
Keim, B.D., Muller, R.A., Stone, G.W., 2004. Spatial and temporal variability of coastal storms in the North Atlantic Basin. Mar. Geol. 210 (1–4), 7–15.
Kent, M., 1982. Plant growth problems in colliery spoil reclamation—a review. Appl. Geogr. 2 (2), 83–107.
Kho, A., Williams, D., 2015. Bulking and Settlement of weakly-cemented and Cemented Coal Mine Spoil.
Langmuir, D., 1997. Aqueous Environmental Geochemistry. Prentice Hall.
Latif, M., Keenlyside, N.S., 2009. El Niño/Southern oscillation response to global warming. Proc. Natl. Acad. Sci. 106 (49), 20578–20583.
Mayes, W., Potter, H., Jarvis, A., 2010. Inventory of aquatic contaminant flux arising from historical metal mining in England and Wales. Sci. Total Environ. 408 (17), 3576–3583.
Miller, B.G., 2015. Fossil Fuel Emissions Control Technologies: Stationary Heat and Power Systems. Butterworth-Heinemann.
Millero, F.J., Lee, K., Roche, M., 1998. Distribution of alkalinity in the surface waters of the major oceans. Mar. Chem. 60 (1), 111–130. https://doi.org/10.1016/S0304-4203(97)00084-4.
Persaud, D., Jaagumagi, R., Hayton, A., 1993. Guidelines for the Protection and Management of Aquatic Sediment Quality in Ontario. Queen's Printer for Ontario. Ministry of Environment and Energy.
Pitman, S.J., Burke, I.T., Jay, H., Cooper, N., Mayes, W.M., Jarvis, A.P., 2024. Long-term coastal dynamics: the evolution of a mixed sediment mega-nourishment consisting of colliery spoil. J. Environ. Manag. 371, 123106.
Pope, N., O'Hara, S., Imamura, M., Hutchinson, T., Langston, W., 2011. Influence of a collapsed coastal landfill on metal levels in sediments and biota—a portent for the future? J. Environ. Monit. 13 (7), 1961–1974.
Riley, A.L., Amezaga, J., Burke, I.T., Byrne, P., Cooper, N., Crane, R.A., Comber, S.D.W., Gandy, C.J., Hudson-Edwards, K.A., Jennings, E., Lewis, E., Lofts, S., MacDonald, J. M., Malcolm, H., Mayes, W.M., Onnis, P., Olszewska, J., Spears, B., Jarvis, A.P., 2022. Incorporating conceptual site models into national-scale environmental risk assessments for legacy waste in the coastal zone [Original Research]. Front. Environ. Sci. 10, 1045482. https://doi.org/10.3389/fenvs.2022.1045482.
Riley, A.L., Cameron, J., Burke, I.T., Onnis, P., MacDonald, J.M., Gandy, C.J., Crane, R. A., Byrne, P., Comber, S., Jarvis, A.P., Hudson-Edwards, K.A., Mayes, W.M., 2024. Environmental behaviour of iron and steel slags in coastal settings. Environ. Sci. Pollut. Control Ser. (31), 42428–42444.
Robins, P.E., Skov, M.W., Lewis, M.J., Giménez, L., Davies, A.G., Malham, S.K., Neill, S. P., McDonald, J.E., Whitton, T.A., Jackson, S.E., 2016. Impact of climate change on UK estuaries: a review of past trends and potential projections. Estuar. Coast Shelf Sci. 169, 119–135.
Rowlatt, S., Lovell, D., 1994. Lead, zinc and chromium in sediments around England and Wales. Mar. Pollut. Bull. 28 (5), 324–329.
Smith, A.M., Hudson-Edwards, K.A., Dubbin, W.E., Wright, K., 2006. Dissolution of jarosite [KFe3 (SO4) 2 (OH) 6] at pH 2 and 8: insights from batch experiments and computational modelling. Geochem. Cosmochim. Acta 70 (3), 608–621.
Tainio, M., de Nazelle, A.J., Götschi, T., Kahlmeier, S., Rojas-Rueda, D., Nieuwenhuijsen, M.J., de Sá, T.H., Kelly, P., Woodcock, J., 2016. Can air pollution negate the health benefits of cycling and walking? Prev. Med. 87, 233–236.
Toimil, A., Camus, P., Losada, I.J., Le Cozannet, G., Nicholls, R.J., Idier, D., Maspataud, A., 2020. Climate change-driven coastal erosion modelling in temperate sandy beaches: methods and uncertainty treatment. Earth Sci. Rev. 202, 103110.
UK Government, 2025. UK pollutant release and transfer register (PRTR) data sets. website: Gov.UK Retrieved from. https://www.gov.uk/guidance/uk-pollutant-release-and-transfer-register-prtr-data-sets.
Vogt, C., 2012. International Assessment of Marine and Riverine Disposal of Mine Tailings. Proceedings of the Secretariat, London Convention/London Protocol, International Maritime Organization, London, England & United Nations Environment Programme-Global Program of Action, London, UK.
Walkden, M., Watson, G., Johnson, A., Heron, E., Tarrant, O., 2016. Coastal catch-up following defence removal at happisburgh. In: Coastal Management: Changing Coast, Changing Climate, Changing Minds. ICE Publishing, pp. 523–532.
Welch, S.A., Kirste, D., Christy, A.G., Beavis, F.R., Beavis, S.G., 2008. Jarosite dissolution II—Reaction kinetics, stoichiometry and acid flux. Chem. Geol. 254 (1–2), 73–86.
Wiggering, H., 1993. Sulfide oxidation—an environmental problem within colliery spoil dumps. Environ. Geol. 22 (2), 99–105.